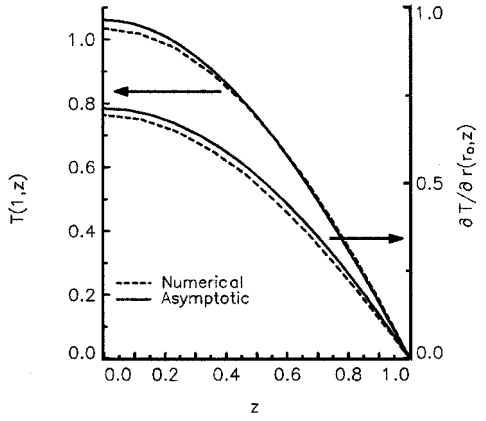

Fig. 2 Comparison of nondimensional free-surface temperature distribution $T(1, z)$ (left), and nondimensional heat flux into the core $\partial T/\partial r(r_0, z)$ (right), for $Ha = 200$ and $r_0 = 0.7879$.

0.7879, 0.7, and 0.5757, respectively. At Ha = 200, 100, 50, the numerical $T(1, 0)$ = 1.0345, 1.0184, 0.9654, and the asymptotic $T(1, 0)$ = 1.06, 1.056, 1.034, which correspond to errors of 2.4, 3.7, and 7.2%, respectively. At Ha = 200, 100, and 50, numerical $\partial T/\partial r(r_0, 0)$ = 0.6947, 0.5871, 0.5355, and the asymptotic $\partial T/\partial r(r_0, 0)$ = 0.7137, 0.6102, 0.4802, which correspond to errors of 2.7, 3.9, and 10.3%, respectively.

Conclusions

Over a large span of magnetic flux densities, we found no periodicity in axisymmetric thermocapillary convection for Pr = 0.0675 for optically heated floating zones. We presented asymptotic solutions for the steady, axisymmetric governing equations that gave errors less than 3% at Ha = 200. The asymptotic solution yielded boundary-layer equations and admitted parameters showing the inertial effects to be proportional to $B^{-3/2}$, where B is the characteristic magnetic flux density, and to be proportional to $L^{1/2}$, where L is the half axial height of the float zone.

Acknowledgments

This research was supported by NASA under Cooperative Research agreement NCC8-90 and by the National Science Foundation under Grant CTS 94-19484.

References

[1]Chang, C. E., and Wilcox W. R., "Inhomogeneities Due to Thermocapillary Flow in Floating Zone Melting," *Journal of Crystal Growth*, Vol. 28, 1975, pp. 8–12.

[2]Robertson, G. D., and O'Connor, D., "Magnetic Field Effects on Float-Zone Si Crystal Growth III. Strong Axial Fields," *Journal of Crystal Growth*, Vol. 76, 1986, pp. 111–122.

[3]Cröll, A., Dold, P., and Benz, K. W., "Segregation in Si Floating-Zone Crystals Grown Under Microgravity and in a Magnetic Field," *Journal of Crystal Growth*, Vol. 137, 1994, pp. 95–101.

[4]Müller, G., and Rupp, R., "The Role of Marangoni Convection in the Growth of GaAs Crystals by the Floating Zone Technique Under Microgravity," *Crystal Properties and Preparation*, Vol. 35, 1991, pp. 138–154.

[5]Series, R. W., and Hurle, D. T. J., "The Use of Magnetic Fields in Semiconductor Crystal Growth," *Journal of Crystal Growth*, Vol. 113, 1991, pp. 305–328.

[6]Khine, Y. Y., Walker, J. S., "Thermocapillary Convection in a Cylinder with a Strong Nonuniform Axisymmetric Magnetic Field," *Journal of Fluid Mechanics*, Vol. 276, 1994, pp. 369–388.

[7]Morthland, T. E., and Walker, J. S., "Convective Heat Transfer Due to Thermocapillary Convection with a Strong Magnetic Field Parallel to the Free Surface," *International Journal of Heat and Mass Transfer*, Vol. 40, No. 14, 1997, pp. 3283–3291.

Experimental Studies of Supersonic Film Cooling with Shock Wave Interaction (II)

Takeshi Kanda* and Fumiei Ono†
National Aerospace Laboratory, Kakuda, Miyagi 981-15, Japan

Introduction

In a previous report,[1] it was shown that the decrease of the film cooling effectiveness in the region of the shock wave/film cooling interaction may not have been caused by mixing of the coolant with the primary gas, but rather by the decrease of the Mach number of the coolant. In the present study, it was confirmed whether or not enhanced mixing occurred. The effectiveness of the film cooling was investigated, and we tried to predict the separation of the film coolant.

Experimental Apparatus and Methods

The testing conditions (except those of the film coolant), and measurement systems were the same as those of the previous tests.[1,2] The gas of the Mach 2.35 primary flow was nitrogen, and the film coolant was argon. The height of the film coolant injector exit was h = 4 mm. The distance downstream of the coolant injector exit is x, and y is the distance from the wall in the test section. Gas sampling was carried out with pitot pressure probes.[2] For the observation of oil flow patterns, silicone oil with titanium dioxide was used. According to the pitot pressure measurement, the Mach number of the coolant M_c was 0.7 ahead of the interaction.[2]

Three kinds of shock generators were used.[2] Table 1 shows the pressure downstream of the shock wave P_3, calculated using the oblique shock wave equations. PO is the total pressure of the primary flow in the wind-tunnel reservoir. The leading edge of the shock generators was located at $x/h = -2.5$. The test condition with no shock generator, i.e., with a 0-deg shock generator, is termed the reference condition.

Results and Discussion

Effectiveness of Film Cooling

Figure 1 shows a spark schlieren photograph and explanations of the flowfield with the shock wave/film cooling interaction. In Table 1, the positions of the shock wave impingement x_{imp}, and the beginning of the expansion-wave impingement from the trailing edge of the shock generator x_{ex}, are listed. Table 1 also lists the positions of the initiation of the interaction x_{int}, and the inflection point in the wall pressure distribution x_{inf}; both were based on the wall pressure P_w distributions (Fig. 2). The measured maximum wall pressures $P_{w,max}/PO$, which are also listed in Table 1, were around 0.12, and they were almost independent of the strength of the incident shock wave, and agreed with the total pressure of the coolant layer.

Figure 3 is the oil flow pattern with the 8-deg shock generator shown by a photograph (bottom) and a sketch (top). In the streamwise direction, the oil gradually accumulated, and then wore off. In the area where oil accumulated, oil flow lines

Presented as Paper 96-2663 at the AIAA/ASME/SAE/ASEE 32nd Joint Propulsion Conference, Lake Buena Vista, FL, July 1–3, 1996; received Dec. 2, 1996; revision received April 11, 1997; accepted for publication April 15, 1997.

*Senior Researcher, Ramjet Propulsion Research Division, Kakuda Research Center. Member AIAA.

†Senior Researcher, Ramjet Propulsion Research Division, Kakuda Research Center.

Table 1 Pressure ratio, and positions of interaction and separation

Deflection angle of shock generator, deg	P_3/PO	$P_{w,max}/PO$	x_{int}/h	x_{inf}/h	x_{imp}/h	x_{ex}/h	x_{si}/h	x_{se}/h	w_s/h	$x_{int,c}/h$	$x_{si,c}/h$
6	0.149	0.118	7.9	——	16.8	24.9	——	——	——	7.8	13.6
7	0.166	0.123	5.4	13	16.1	24.6	13.3	17.8	0.36	6.0	12.5
8	0.185	0.125	2.5	13	14.9	23.2	11.3	17.5	0.44	3.0	10.0

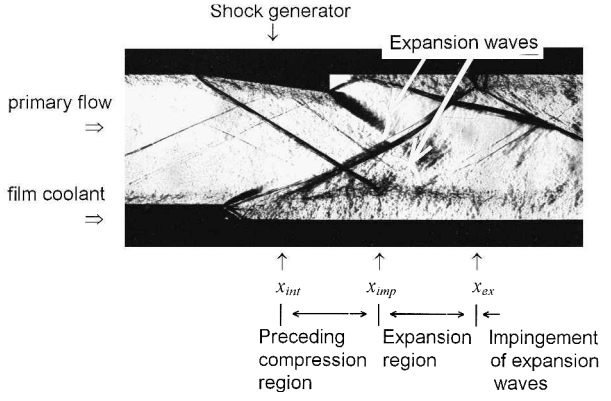

Fig. 1 Spark schlieren photograph of the flowfield with the shock wave/film cooling interaction by 8-deg shock generator.

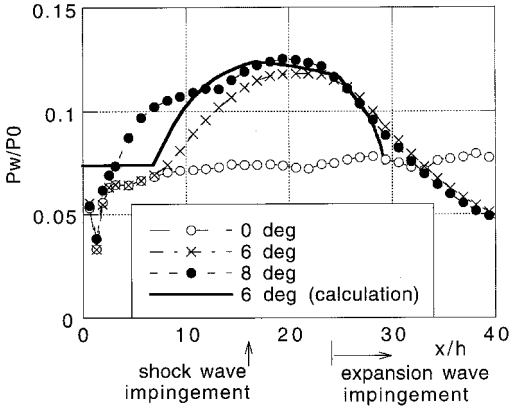

Fig. 2 Wall pressure distribution.

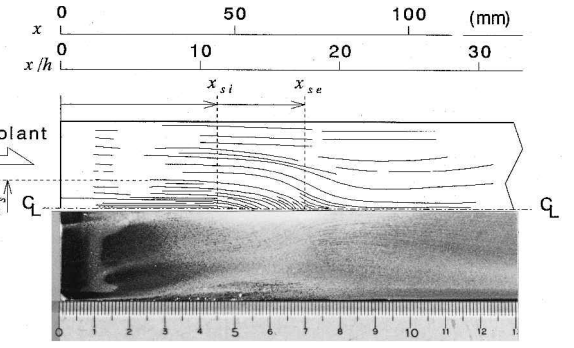

Fig. 3 Oil flow pattern using 8-deg shock generator.

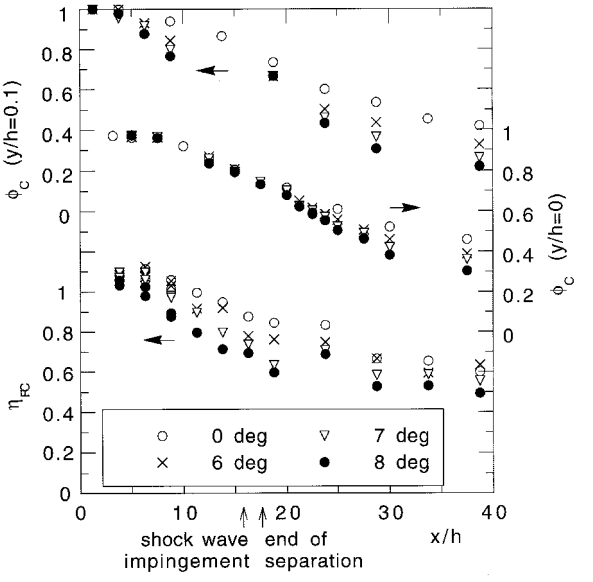

Fig. 4 Mole fractions of coolant gas on the wall surface (y/h = 0) and at y/h = 0.1, and film cooling effectiveness.

turned toward the centerline from both sides, meaning that separation occurred. Downstream of the separation, oil flow lines turned and became parallel to the centerline. There was no trace of reattachment of the separation, meaning that the separated boundary layer of the film coolant was lifted up and mixed with the core part of the film coolant. Such separation did not occur when the 6-deg shock generator was used. Table 1 lists the initial point and the endpoint of the separation on the centerline, x_{si} and x_{se}, and the width of the coolant layer that separates downstream w_s.

Figure 4 shows the mole fractions of the coolant ϕ_c, at y/h = 0 and 0.1, and the film cooling effectiveness η_{FC}. The effectiveness is defined by

$$\eta_{FC} = (t_{aw} - TO_\infty)/(TO_c - TO_\infty) \quad (1)$$

where t_{aw}, TO_∞, and TO_c are the measured wall temperature, the total temperature of the primary flow, and the total temperature of the coolant,[2] respectively. When there was a shock wave impingement, ϕ_c at y/h = 0.1 became lower than that of the reference condition. On the wall surface, however, ϕ_c was almost the same as or a little lower than that of the reference condition, meaning that the mixing was very small on the wall. Therefore, the decrease of η_{FC} for $x/h < 20$ was caused by the decrease in M_c, which is in agreement with Ref. 1. This also agrees with the observations that there was both an active and a passive region of mixing in the wall jet,[3] and that the turbulence did not increase because of the shock wave impingement near the wall.[4] The observation of effective film cooling, even with burning in the shear layer,[5] may also indicate very small mixing on the wall.

Even though separation occurred, ϕ_c at y/h = 0 and η_{FC} decreased gradually downstream of the separation for $x/h >$ 20. This change seems to be related to the structure of the separation; the coolant flowed downstream of the separation from both sides (Fig. 3). The present results are not consistent with the results of Juhany and Hunt[6]; i.e., the change in the recovery temperature was large when there was separation. The difference between our results and those of Ref. 6 seems to be because of the difference in the separation structure.

Prediction of Separation of Film Coolant

Prediction of the coolant separation is necessary for the design of a film cooling system. The following procedure was used to predict the separation. First, the relation between the mass transfer and the momentum transfer was investigated. Second, based on this result, a flow structure model was constructed to predict the wall pressure distribution. Finally, we

attempted to predict the separation of the coolant, using the calculated pressure distribution.

Momentum Transfer

A mixing model was constructed to investigate the role of mass transfer in the momentum transfer mechanism (upper right side of Fig. 5). The model has the following features.

1) There are two inviscid flows, i.e., the coolant and the boundary-layer flows of the primary flow. Initially, they are at the same static pressure.

2) The mean properties of the boundary-layer flow are calculated, assuming the 1/7th power law for the velocity distribution and the Crocco–Busemann relation for the temperature profile. For example, the mean velocity u_b, is calculated from

$$u_b = \frac{\int^{\delta} (\rho u^2)\, dy}{\int^{\delta} (\rho u)\, dy} \tag{2}$$

where δ and ρ are boundary-layer thickness and density, respectively.

3) The coolant flows parallel to the boundary layer, and is then fully mixed with it.

4) The cross section of the mixed flow A_{mix} is equal to the sum of those of the coolant flow A_c, the boundary layer flow A_b, and the separating plate A_p; i.e., $A_{mix} = A_c + A_b + A_p$.

5) The pressure acting on the end of the separating plate is taken as 0.2 times P_b from the turning angle of the primary flow in the schlieren picture.

The conservation equations were as follows:

$$\rho_{mix} u_{mix} A_{mix} = \rho_c u_c A_c + \rho_b u_b A_b \tag{3}$$

$$\rho_{mix} u_{mix}^2 A_{mix} + P_{mix} A_{mix} = (\rho_c u_c^2 A_c + P_c A_c) + (\rho_b u_b^2 A_b + P_b A_b) + P_p A_p \tag{4}$$

$$\rho_{mix} u_{mix} A_{mix} \left(\frac{1}{2} u_{mix}^2 + \frac{\gamma_{mix}}{\gamma_{mix} - 1} \frac{P_{mix}}{\rho_{mix}} \right) = \rho_c u_c A_c \times \left(\frac{1}{2} u_c^2 + \frac{\gamma_c}{\gamma_c - 1} \frac{P_c}{\rho_c} \right) + \rho_b u_b A_b \left(\frac{1}{2} u_b^2 + \frac{\gamma}{\gamma - 1} \frac{P_b}{\rho_b} \right) \tag{5}$$

Here, $P = \rho RT$, and γ and R are, respectively, the ratio of specific heats and gas constant. When the properties at the upstream boundary are specified, a quadratic equation is derived from the three simultaneous equations. One set of the solutions is for subsonic flow.

Figure 5 shows the relationship between the mole fraction of the primary fluid ϕ_∞, and the local total pressure po. The subsonic solution agreed with the measured values, meaning that the transfer of momentum from the primary flow to the coolant was principally because of mixing; in other words, the viscous effects were very small.

Pressure Distribution

The mechanism of the shock wave/film cooling interaction with no separation may be explained as follows (Fig. 1). The primary flow travels through two shock waves (one from the shock generator and one from the preceding compression region). Because the coolant layer does not have the pressure increase by the shock wave from the shock generator, the pressure in the coolant is lower than that in the primary flow when the primary flow is parallel to the wall through the shock waves. Therefore, expansion waves emanate from the point of the shock wave impingement, and the primary flow turns downward. Then the expansion waves from the trailing edge

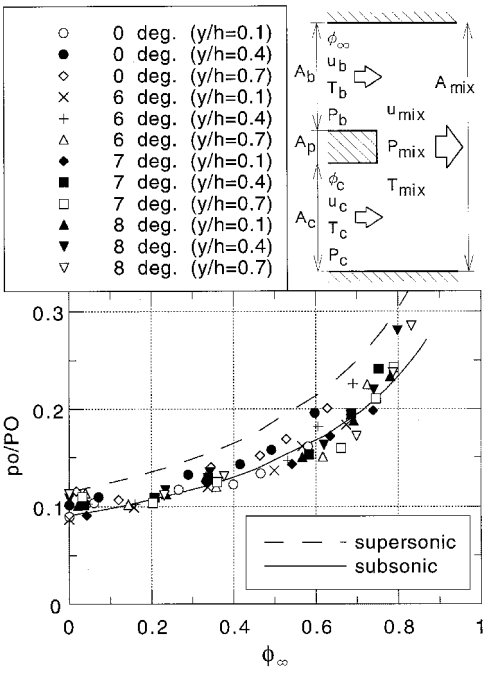

Fig. 5 Relation between the local total pressure and the primary gas mole fraction.

of the shock generator impinges on the coolant layer, and the primary flow gradually changes its direction parallel to the wall. The coolant layer thins until choking occurs.

Based on the previous observation, a flow structure model was constructed to predict the wall pressure distribution. The calculation methods and assumptions are as follows:

1) The coolant layer is one dimensional, while the primary flow is two dimensional.

2) According to the small viscous effects, the primary flow and the coolant are inviscid.

3) There is no mixing between the primary flow and the coolant. The initial Mach number of the coolant was taken as 0.9 instead of 0.7, to simulate the increase of the total pressure because of mixing. The coolant contained 10% nitrogen, which was the mean value in the interacting region.

4) The position of the shock wave impingement and its strength are specified. The starting position of the expansion wave impingement on the coolant layer is also specified.

In the calculation procedure, first the initial point of interaction $x_{int,c}$ is assumed. Then the properties are calculated, maintaining the pressure balance between the primary flow and the coolant. Finally, the choking condition is checked (primary flow parallel to the wall, and coolant sonic). Figure 2 shows the calculated wall pressure for the 6-deg shock generator, and the value of $x_{int,c}$ was in good agreement with that listed in Table 1; meaning that the wall pressure distribution was determined by the interaction of the subsonic coolant with the supersonic primary flow, and that the increase in the wall pressure was mainly because of the deceleration of the coolant layer.

Prediction of Separation

The separation of the coolant layer was investigated using the formula of White[7] for a subsonic, turbulent boundary layer and the calculated pressure distribution. The coolant was assumed to contain 10% nitrogen. The representative length, necessary in the formula of White,[7] was the distance from the coolant injector exit to the point $x_{int,c}$. The numerical results are listed in Table 1. The calculated separation positions $x_{si,c}$, with the 7- and 8-deg shock generators, agreed with x_{si} by the oil flow tests. Though separation occurs with the 6-deg shock generator in the calculation, $x_{si,c}$ was smallest.